1. THE MOMENT-BASED LOW-ORDER EQUATIONS

The formation of the LO equations is similar to a discontinuous FE method. Weighted integrals of the the equations are taken with functions that have local support as weight functions. The equations are written with element-wise moments of I and T as unknowns. Leaving the solution in this form allows for use of information form a previous HO solution to eliminate auxillary unknowns from the equations. This is different than a standard Galerkin FE method [**?**] where a functional form of the solution is directly assumed. The final equations will have a similar form to S_2 equations, but we have not used a collocation method in angle, which should limit ray effects [**?**] in higher spatial dimensions. The equations eliminate extra spatial unknowns in a manner similar to to a linear-discontinuous FE method [**?**]. We also explore the possibility of using the MC solution to modify the discretization of the LO solution in Sec. **??**. MOVE

The remainder of this chapter is structured as follows: the general moments will be derived and then the angular and spatial closure are discussed REWRITE. For simplicity, the implicit Euler discretization is used throughout this section. Sec. **??** will use the HO solution and MC transport to consistently close the equations in time, improving time accuracy.

1.1 Forming the Space-Angle Moment Equations

1.1.1 LO Spatial mesh and Finite-Element Spatial Moments

The LO equations are formulated over a FE mesh. The domain for the i-th spatial element (or cell) has support $x \in [x_{i-1/2}, x_{i+1/2}]$ with width $h_i = x_{i+1/2} - x_{i-1/2}$ and cell center $x_i = x_{i-1/2} + h_i/2$. There is a total of N_c elements, spanning the spatial domain $0 \leq x \leq X$. For simplicity, this spatial mesh is fixed throughout the

simulation. Mesh adaptation is only applied in the HO solver.

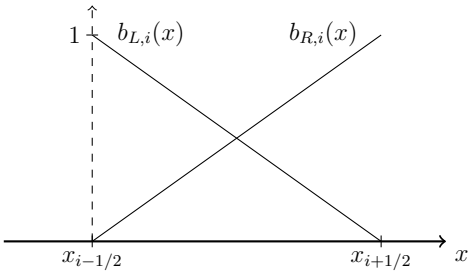

Figure 1.1: Illustration of linear finite element basis functions $b_{L,i}(x)$ and $b_{R,i}(x)$ for spatial element i.

The spatial moments are defined by integrals weighted with the standard linear finite element (FE) interpolatory basis functions. An illustration of the two linear FE basis functions for the i-th element is given in Fig. 1.1. The left basis function is defined as

$$b_{L,i}(x) = \begin{cases} \frac{x_{i+1/2}-x}{h_i} & x_{i-1/2} \leq x \leq x_{i+1/2} \\ 0 & \text{elsewhere} \end{cases}, \tag{1.1}$$

corresponding to the node $x_{i-1/2}$. The right basis function is

$$b_{R,i}(x) = \begin{cases} \frac{x-x_{i-1/2}}{h_i} & x_{i-1/2} \leq x \leq x_{i+1/2} \\ 0 & \text{elsewhere} \end{cases}, \tag{1.2}$$

corresponding to the node $x_{i+1/2}$. With these definitions, a local linear approximation to a function f can be formulated as $f(x) \simeq f_{L,i} b_{L,i}(x) + f_{R,i} b_{R,i}(x), \quad x \in [x_{i-1/2}, x_{i+1/2}]$.[1]

[1] In literature the FE functions are formally defined with support over two adjacent elements. However, in our notation our functions only have non-zero support in element i. This accommodates our later definition of moments and discontinuous unknowns.

The spatial moments are defined by integrals over the each element, using the two basis functions. We use $\langle\cdot\rangle$ to indicate integration over a spatial element. The spatial moments are

$$\langle\cdot\rangle_{L,i} = \frac{2}{h_i}\int_{x_{i-1/2}}^{x_{i+1/2}} b_{L,i}(x)(\cdot)\mathrm{d}x \tag{1.3}$$

and

$$\langle\cdot\rangle_{R,i} = \frac{2}{h_i}\int_{x_{i-1/2}}^{x_{i+1/2}} b_{R,i}(x)(\cdot)\mathrm{d}x. \tag{1.4}$$

where the factor of $2/h_i$ is a normalization constant. It is noted in this notation $\langle\phi\rangle_{L,i}$ and $\langle\phi\rangle_{R,i}$ represent spatial moments of the intensity over cell i, opposed to $\phi_{L,i}$ and $\phi_{R,i}$, which represent the interior value of the linear representation of $\phi(x)$ at $x_{i-1/2}$ and $x_{i+1/2}$ within the cell.

To simplify notation and discussion, we also define the slope and average moments over a spatial cell. The average scalar intensity is

$$\phi_i = \frac{1}{h_i}\int_{x_{i-1/2}}^{x_{i+1/2}} \phi(x)\mathrm{d}x \tag{1.5}$$

and

$$\phi_{x,i} = \frac{6}{h_i}\int_{x_{i-1/2}}^{x_{i+1/2}} \left(\frac{x-x_i}{h_i}\right)\phi(x)\mathrm{d}x. \tag{1.6}$$

The linear representation over a cell in terms of these moments is $\phi(x) = \phi_i + 2/h_i^2\phi_x(x-x_i)$, for $x \in (x_{i-1/2}, x_{i+1/2})$.

1.1.2 Definition of Angular Moments

To reduce the angular dimensionality, positive and negative half-range integrals of the angular intensity are taken. The half-range integrals of I are defined as $\phi^+(x) = 2\pi\int_0^1 I(x,\mu)\,\mathrm{d}\mu$ and $\phi^-(x) = 2\pi\int_{-1}^0 I(x,\mu)\,\mathrm{d}\mu$, respectively. Thus, in terms of half-range quantities, the mean intensity is $\phi(x) = \phi^-(x) + \phi^+(x)$.

1.1.3 Space-Angle Moments of the Transport Equation

The LO radiation equations are formed by applying the space and angle moment operators to the transport equation and performing algebraic manipulation. Application of the L moment operator to the time-discretized transport equation, i.e., Eq. (**??**), yields

$$-2\mu_{i-1/2}I_{i-1/2}^{n+1}+\frac{1}{h_i}\int_{x_{i-1/2}}^{x_{i+1/2}}\mu I^{n+1}\mathrm{d}x+\left(\sigma_{t,i}^{n+1}+\frac{1}{c\Delta t}\right)h_i\langle\phi\rangle_{L,i}^{n+1,+} \\ -\frac{\sigma_{s,i}h_i}{2}\left(\langle\phi\rangle_{L,i}^{n+1,+}+\langle\phi\rangle_{L,i}^{n+1,-}\right)=\frac{h_i}{2}\langle\sigma_a^{n+1}acT^{n+1,4}\rangle_{L,i}+\frac{h_i}{c\Delta t}\langle\phi\rangle_{L,i}^{n,+}. \quad (1.7)$$

Here, the cross sections have been assumed constant over a cell and the mean intensity has been expanded in terms of the half-range unknowns. REWRITE: ADD USEFUL RELATIONS BETWEEN THE MOMENTS TO THE APPENDIX The relation in Eq. (**??**) is used to eliminate the integral from the equation is terms of L and R moments.

The resulting equation is integrated over the positive half range:

$$-2\mu_{i-1/2}I_{i-1/2}^{n+1}+\frac{1}{h_i}\int_{x_{i-1/2}}^{x_{i+1/2}}\mu I^{n+1}\mathrm{d}x+\left(\sigma_{t,i}^{n+1}+\frac{1}{c\Delta t}\right)h_i\langle\phi\rangle_{L,i}^{n+1,+} \\ -\frac{\sigma_{s,i}h_i}{2}\left(\langle\phi\rangle_{L,i}^{n+1,+}+\langle\phi\rangle_{L,i}^{n+1,-}\right)=\frac{h_i}{2}\langle\sigma_a^{n+1}acT^{n+1,4}\rangle_{L,i}+\frac{h_i}{c\Delta t}\langle\phi\rangle_{L,i}^{n,+}. \quad (1.8)$$

1.1.4 Radiation Energy Equations

Pairwise application of the L and R basis moments with the $+$ and $-$ half-range integrals to Eq. (**??**) ultimately yields four moment equations per cell. As in [28], algebraic manipulation is performed to form intensity-weighted averages of μ, which we denote as consistency terms. As an example, the equation resulting from

application of the L moment and positive half-range integral is

$$-2\mu_{i-1/2}^{n+1,+}\phi_{i-1/2}^{n+1,+}+\{\mu\}_{L,i}^{n+1,+}\langle\phi\rangle_{L,i}^{n+1,+}+\{\mu\}_{R,i}^{n+1,+}\langle\phi\rangle_{R,i}^{n+1,+}+\left(\sigma_{t,i}^{n+1}+\frac{1}{c\Delta t}\right)h_i\langle\phi\rangle_{L,i}^{n+1,+}$$
$$-\frac{\sigma_{s,i}h_i}{2}\left(\langle\phi\rangle_{L,i}^{n+1,+}+\langle\phi\rangle_{L,i}^{n+1,-}\right)=\frac{h_i}{2}\langle\sigma_a^{n+1}acT^{n+1,4}\rangle_{L,i}+\frac{h_i}{c\Delta t}\langle\phi\rangle_{L,i}^{n,+}, \quad (1.9)$$

where the $\phi_{i-1/2}^{+}$ and $\mu_{i-1/2}^{+}$ terms represent face-averaged quantities at $x_{i-1/2}$. The negative direction and R moment equations are derived analogously. The element-averaged angular consistency terms are defined in terms of half-range integrals, e.g.,

$$\{\mu\}_{L,i}^{n+1,+}\equiv\frac{\langle\mu I^{n+1}\rangle_{L,i}^{+}}{\langle I^{n+1}\rangle_{L,i}^{+}}=\frac{\frac{2}{h_i}\int_0^1\int_{x_{i-1/2}}^{x_{i+1/2}}\mu\, b_{L,i}(x)I^{n+1}(x,\mu)\mathrm{d}x\mathrm{d}\mu}{\frac{2}{h_i}\int_0^1\int_{x_{i-1/2}}^{x_{i+1/2}}b_{L,i}(x)I^{n+1}(x,\mu)\mathrm{d}x\mathrm{d}\mu}. \quad (1.10)$$

The $\mu_{i-1/2}^{n+1,+}$ term is defined analogously and represents an angular average on the face at $x_{i-1/2}$.

1.1.5 Material Energy Equations

To derive the LO material energy equations, $T(x)$ is represented spatially in the LDFE trial space, i.e., $T(x)\simeq T_{L,i}b_{L,i}(x)+T_{R,i}b_{R,i}(x), \quad x\in(x_{i-1/2},x_{i+1/2})$. Similarly, the emission term is represented in the material and radiation equations with the LDFE interpolant $T^4(x)\simeq T_{L,i}^4b_{L,i}(x)+T_{R,i}^4b_{R,i}(x)$. The L and R spatial moments are taken of the material energy equations; the LDFE representations for $T(x)$ and $\sigma_acT^4(x)$ are used to simplify the spatial integrals. For example, the final LO material energy equation resulting from application of the L moment is

$$\frac{\rho_ic_{v,i}}{\Delta t}\left[\left(\frac{2}{3}T_{L,i}+\frac{1}{3}T_{R,i}\right)^{n+1}-\left(\frac{2}{3}T_{L,i}+\frac{1}{3}T_{R,i}\right)^{n}\right]+\sigma_{a,i}^{n+1}\left(\langle\phi\rangle_{L,i}^{+}+\langle\phi\rangle_{L,i}^{-}\right)^{n+1}$$

$$= \sigma_{a,i}^{n+1} ac \left(\frac{2}{3} T_{L,i}^4 + \frac{1}{3} T_{R,i}^4 \right)^{n+1} . \quad (1.11)$$

Cross sections have been assumed constant over each element, evaluated at the average temperature within the element, i.e., $\sigma_{a,i}^{n+1} = \sigma_{a,i}([T_{L,i}^{n+1} + T_{R,i}^{n+1}]/2)$. Because the material energy balance only contains angularly integrated quantities, there is no need to take angular moments of the above equation.

1.2 Closing the System with Information from the HO solution

The six degrees of freedom (DOF) over each cell i are the four moments $\langle\phi\rangle_{L,i}^{+}$, $\langle\phi\rangle_{R,i}^{+}$, $\langle\phi\rangle_{L,i}^{-}$, and $\langle\phi\rangle_{R,i}^{-}$ and the two spatial edge values $T_{L,i}$ and $T_{R,i}$. The four radiation and two material energy equations define a system of equations for the six DOF, coupled to other cells via upwinding in the streaming term. The relation between the volume and face averaged quantities and the angular consistency parameters (e.g., Eq. (1.10)) are not known a priori. A lagged estimate of I^{n+1} from the previous HO solve is used to estimate the angular consistency parameters. In the HOLO algorithm, the equations for LO unknowns at iteration $k+1$ use consistency parameters computed (via relations, e.g., Eq. (1.10)) using the latest HO solution $\tilde{I}^{n+1,k+1/2}$ as an approximation for $I^{n+1}(x,\mu)$. To close the LO system spatially, a linear-discontinuous (LD) spatial closure with the usual upwinding approximation is used. For example, for positive flow (e.g., Eq. (1.9)) the face terms $\mu_{i-1/2}$ and $\phi_{i-1/2}$ are upwinded from the previous cell $i-1$ or from a boundary condition; the terms at $x_{i+1/2}$ are linearly extrapolated, computed using the L and R basis moments, e.g., $\phi_{i+1/2}^{+} = 2\langle\phi\rangle_{R}^{+} - \langle\phi\rangle_{L}^{+}$. Because there are no derivatives of T in Eq. (**??**), there is no need to define T on the faces; the temperature has been assumed linear within a cell to relate T and T^4.

The choice of a LD spatial closure should preserve the equilibrium diffusion limit.

In this limit, the MC HO solution will estimate angular consistency terms associated with an isotropic intensity, based on a spatially LD emission source. The isotropic-intensity consistency terms will produce LO equations that are equivalent to S_2 equations, with quadrature points of $\pm 1/2$. Because the spatial closure produces equations that are equivalent to an LDFE solution to these equations, we expect the equations to preserve the equilibrium diffusion limit [18, 4].

The linear-discontinuous (LD) closure with upwinding is not strictly positive. In particular, for optically thick cells with a steep intensity gradient, the solution becomes negative. These negative values of intensity can propagate to adjacent cells. In thick regions of TRT problems, reasonably fine spatial cells can still be on the order of millions of mean free paths; negative values with an LD representation are unavoidable in practice for such cells and mesh refinement is of minimal use. Typically, for a standard LDFE method, the equations are lumped to produce a strictly positive solution (for 1D) [18]. However, standard FE lumping procedures would introduce difficulties in computing the consistency terms from the HO solution. Thus, an alternative spatial closure is used that is equivalent to the standard FE lumping procedure. The L and R moments are defined the same as before, preserving the average within a cell, but the relation between the moments and the outflow is modified. For example, for positive μ, the outflow is now defined as $\phi^+_{i+1/2} = \langle \phi \rangle^+_R$. Because the basis function $b_{R,i}(x)$ is strictly positive, the outflow is positive. This closure is only used in cells where negative intensities occur.

1.2.1 Newton's Method for LO Equations

Adding the equations for each cell together forms a global system of coupled equations. The equations are nonlinear due to the Planckian emission source. We have used Newton's method to solve the nonlinear system, based on a typical linearization

of the Planckian source with cross sections evaluated at temperatures from the previous iteration, as described in [18]. Because we have only considered problems with constant densities and heat capacities, the linearization described below is in terms of temperature T rather than material internal energy, for simplicity. However, the linearization can be formed in terms of internal energy to apply this method to a general equation of state.

To formulate the Newton iterations, the Planckian source is linearized in the material and radiation equations (Eq. (**??**) & Eq. (**??**)). Application of the first order Taylor expansion in time to the implicit emission source $B(T^{n+1})$, about some temperature T^* at some time $t^* \in [t^n, t^{n+1}]$, yields

$$\sigma_a^{n+1} acT^{4,n+1} \simeq \sigma_a^* ac \left[T^{*4} + (T^{n+1} - T^*)4T^{*3}\right] \tag{1.12}$$

where $\sigma_a^* \equiv \sigma_a(T^*)$. Substitution of this expression into Eq. (**??**) yields

$$\rho c_v \left(\frac{T^{n+1} - T^n}{\Delta t}\right) = \sigma_a^* \phi^{n+1} - \sigma_a^* ac \left[T^{*4} + (T^{n+1} - T^*)4T^{*3}\right]. \tag{1.13}$$

Algebraic manipulation of this equation yields an expression for $T^{n+1} - T^*$:

$$\left(T^{n+1} - T^*\right) = \frac{\frac{\sigma_a^* \Delta t}{\rho c_v}\left[\phi^{n+1} - acT^{*4}\right] + (T^n - T^*)}{1 + \sigma_a^* ac\Delta t \frac{4T^{*3}}{\rho c_v}}.$$

This expression is substituted back into Eq. (1.12) to form an explicit approximation for the emission source at t^{n+1} as

$$\sigma_a acT^{4,n+1} \simeq \sigma_a^*(1 - f^*)\phi^{n+1} + f^* \sigma_a^* acT^{4,n} + \rho c_v \frac{1 - f^*}{\Delta t}(T^n - T^*) \tag{1.14}$$

where $f^* = [1 + \sigma_a^* c\Delta t 4aT^{*3}/(\rho c_v)]^{-1}$ is often referred to as the Fleck factor [8].

Next, the above equation must be spatially discretized. Application of the L spatial moment yields

$$\langle \sigma_a^* acT^{4,n+1} \rangle_{L,i} = \sigma_{ai}^*(1 - f_i^*)\langle \phi^{n+1} \rangle_{L,i} + f_i^* \sigma_{ai}^* ac \left(\frac{2}{3} T_{L,i}^{4,n} + \frac{1}{3} T_{R,i}^{4,n} \right) \\ \rho_i c_{vi} \frac{1 - f_i^*}{\Delta t} \left[\frac{2}{3} \left(T_{L,i}^n - T_{L,i}^* \right) + \frac{1}{3} \left(T_{R,i}^n - T_{R,i}^* \right) \right], \quad (1.15)$$

where $T^{4,n}$ and T^n have been assumed LD and f^* is assumed constant over a cell, i.e., $f_i^* \equiv \sigma_a(T_i^*)$. The error introduced by a constant f^* approaches zero as the non-linearity is converged because T^* approaches T^{n+1}. Based on an estimate for T^*, Eq. (1.15) is an expression for the Planckian emission source in the radiation moment equations with an additional effective scattering source. A similar expression can be derived for $\langle \sigma_{a,i} acT^4 \rangle_R$ and the right moment equations. The expressions for the emissions source is substituted into the radiation moment equations (Eq. (1.9)– (**??**)) to produce a linear system of equations for the new radiation intensity moments.

Once the linear equations have been solved for new radiation moments, new temperature unknowns can be estimated. To conserve energy, the same linearization and discretizations used to solve the radiation equation must be used in the material energy equation. Substitution of Eq. (1.15) into the material energy L moment equation ultimately yields

$$\frac{2}{3} T_{L,i}^{n+1} + \frac{1}{3} T_{R,i}^{n+1} = \frac{f_i^* \sigma_{ai}^* \Delta t}{\rho c_v} \left[\langle \phi^{n+1} \rangle_{L,i} - ac \left(\frac{2}{3} T_{L,i}^{4,n} + \frac{1}{3} T_{R,i}^{4,n} \right) \right] + \\ (1 - f_i^*) \left(\frac{2}{3} T_{L,i}^* + \frac{1}{3} T_{R,i}^* \right) + f \left(\frac{2}{3} T_{L,i}^n + \frac{1}{3} T_{R,i}^n \right) \quad (1.16)$$

A similar expression is produced for the R moment equation. This produces a local

matrix equation to solve for new T unknowns. If both the radiation and temperature unknowns are lumped, this matrix becomes diagonalized.

Based on these equations, the algorithm for solving the LO equations, with iteration index l, is defined as

1. Initialize T unknowns using T^n or the last estimate of T^{n+1} from previous LO solve

2. Build the LO system based on the effective scattering $(1 - f^l)$ and emission terms evaluated using T^l.

3. Solve the linearized LO system to produce an estimate for $\phi^{n+1,l}$.

4. Evaluate a new estimate of T^{n+1} unknowns using Eq. (1.16).

5. $T^* \leftarrow \tilde{T}^{n+1}$.

6. Repeat 2-5 until $(T^{n+1,k})^4$ and $\phi^{n+1,k}$ are converged.

1.2.2 Direct Solution of the LO Equations

Isotropic scattering, including effective scattering terms from the linearization, are included in the system matrix. The system matrix is an asymmetric, banded matrix with a band width of seven and is inverted directly. Newton iterations are repeated until $\phi^{n+1}(x)$ and $T^{n+1}(x)$ are converged to a desired relative tolerance. Convergence is calculated using the spatial L_2 norm of the change in $\phi^{n+1}(x)$ and $T^{n+1}(x)$, relative to the norm of each solution. The lumping-equivalent discretization discussed above is used for cells where the solution for ϕ^{n+1} becomes negative. When negative values for $\phi^{n+1,\pm}(x)$ are detected, the lumping-equivalent discretization is used within those cells and that Newton step is repeated.

2. ACCELERATED ITERATIVE SOLUTION TO THE LO EQUATIONS

2.1 Diffusion Synthetic Acceleration of the LO Equations

As described in Sec. **??**, the fully-discretized LO equations can include the scattering term in the system matrix. This allows for the system to be directly inverted. However, the S_2 like system cannot be efficiently inverted directly in higher spatial dimensions. To demonstrate a possible path forward in higher dimensions, we will investigate the use of a standard source iteration scheme to solve the LO equations. As material properties become more diffusive (e.g., c_v is small and σ_a is large), the effective scattering source becomes large. This results in a spectral radius of the source iterations that approaches unity [18]. These regimes are typical in TRT simulations, so an acceleration method is critical. We will accelerate the source iterations with a nearly-consistent diffusion synthetic acceleration (DSA) method [24, 23].

We can perform standard source iterations by lagging the scattering source in the LO equations, which uncouples unknowns between the two half-ranges. This produces a lower-triangular system where the spatial unknowns can be determined sequentially along the two directions of flow via a standard sweeping procedure [16, 18]. The newly computed half-range intensities can be used to compute the scattering source for the next iteration. This process is repeated until convergence. A form of DSA referred to as the WLA method is used to accelerate the source iterations [24]. Between each source iteration, a residual equation is formed that provides the error in the current scattering iteration. The DSA method uses an approximate, lower-order operator to estimate the error in the zeroth angular moment of the intensity. The DSA equations can be more efficiently solved than the S_2-like sweeps that are being accelerated, but will accurately resolve the slowly converging diffusive error modes.

It is important for the spatial discretization of the DSA equations to be closely related to the discretization of the LO equations for the acceleration to be effective. The WLA method first solves a spatially-continuous discretization of the diffusion equation for the iterative error on faces. The error on the faces is then mapped onto the volumetric moment unknowns via a LD discretization of diffusion equation [24]. The LD mapping resolves issues that would occur in optically-thick cells, while the continuous diffusion equation is accurate in the EDL where acceleration is important.

We have implemented the DSA algorithm and initial results indicate that the acceleration is effective. However, we have only considered the case when the LO equations and DSA equations are lumped. We will investigate the effect of acceleration when alternative negativity fix-ups are implemented that result in DSA and LO equations that are not spatially consistent. We will recast the DSA method as a preconditioner to an iterative Krylov solution [7] of the LO equations if acceleration degrades. Generally, Krylov methods mitigate acceleration losses due to inconsistencies in the acceleration method. In higher dimensions, the use of a Krylov method is necessary for effective acceleration for nearly-consistent acceleration methods such as WLA in problems with mixed optical thicknesses [7], e.g., typical radiative transfer problems. We would apply the preconditioned-Krylov approach to allow for the use of lumped DSA equations as a preconditioner, with the LO equations using one of the other fixup approaches detailed in the previous section. It is noted we are not interested in measuring the reduction of computational time because in 1D the LO equations can be directly solved efficiently. We are just interested in ensuring that DSA or a preconditioned-Krylov methods can reduce the number of scattering iterations sufficiently, including cases where inconsistencies in the LO equations are present.

2.2 Diffusion Synthetic Acceleration

To accelerate source iteration in the LO system, a version of WLA DSA is used. The following derivations are to solve a diffusion equation which can be used to compute the source iteration error in the LO sweeps.

2.2.1 Forming a Continuous Diffusion Equation

Beginning with the P_1 equations for a steady-state problem

$$\frac{\partial J}{\partial x} + \sigma_a \phi = Q \tag{2.1}$$

$$\sigma_t J + \frac{1}{3}\frac{\partial \phi}{\partial x} = 0 \tag{2.2}$$

$$\tag{2.3}$$

spatial finite element moments are taken. The spatial moments are defined as

$$\langle \cdot \rangle_L = \frac{2}{h_i} \int_{x_{i-1/2}}^{x_{i+1/2}} \mathrm{d}x \, b_{L,i}(x) \, (\cdot) \tag{2.4}$$

$$\langle \cdot \rangle_R = \frac{2}{h_i} \int_{x_{i-1/2}}^{x_{i+1/2}} \mathrm{d}x \, b_{R,i}(x) \, (\cdot) \, . \tag{2.5}$$

where $b_{L,i}(x) = (x_{i+1/2} - x)/h_i$ and $b_{R,i}(x) = (x - x_{i-1/2})/h_i$. The scalar flux ϕ will ultimately be assumed continuous at faces. The scalar flux is assumed linear on the interior of the cell, i.e., $\phi(x) = \phi_L b_L(x) + \phi_R b_R(x)$, for $x \in (x_{i-1/2}, x_{i+1/2})$. Taking the left moment, evaluating integrals, and rearranging yields

$$J_i - J_{i-1/2} + \frac{\sigma_{a,i} h_i}{2} \left(\frac{2}{3}\phi_{L,i} + \frac{1}{3}\phi_{R,i} \right) = \frac{h_i}{2} \langle q \rangle_{L,i} \ , \tag{2.6}$$

where J_i is the average of the current over the cell. The moments of q are not simplified to be compatible with the LO moment equations. For the R moment

$$J_{i+1/2} - J_i + \frac{\sigma_{a,i}h_i}{2}\left(\frac{2}{3}\phi_{L,i} + \frac{1}{3}\phi_{R,i}\right) = \frac{h_i}{2}\langle q\rangle_{R,i} \ . \tag{2.7}$$

The equation for the L moment is evaluated for cell $i+1$ and added to the R moment equation evaluated at i. The current is assumed continuous at $i+1/2$ to eliminate the face current from the system. The sum of the two equations becomes

$$J_{i+1} - J_i + \frac{\sigma_{a,i+1}h_{i+1}}{2}\left(\frac{2}{3}\phi_{L,i+1} + \frac{1}{3}\phi_{R,i+1}\right) + \frac{\sigma_{a,i}h_i}{2}\left(\frac{1}{3}\phi_{L,i} + \frac{2}{3}\phi_{R,i}\right) = \frac{h}{2}\left(\langle q\rangle_{L,i+1} + \langle q\rangle_{R,i}\right). \tag{2.8}$$

The scalar flux is assumed continuous at each face, i.e., $\phi_{L,i+1} = \phi_{R,i} \equiv \phi_{i+1/2}$. We then approximate the cell-averaged currents with Fick's law as

$$J_i = -D_i\frac{\phi_{i+1/2} - \phi_{i-1/2}}{h_i}. \tag{2.9}$$

Combining the definition and rearranging yields the following discrete diffusion equation:

$$\left(\frac{\sigma_{a,i+1}h_{i+1}}{6} - \frac{D_{i+1}}{h_{i+1}}\right)\phi_{i+3/2} + \left(\frac{D_{i+1}}{h_{i+1}} + \frac{D_i}{h_i} + \frac{\sigma_{a,i+1}h_{i+1}}{3} + \frac{\sigma_{a,i}h_i}{3}\right)\phi_{i+1/2} + \left(\frac{\sigma_{a,i}h_i}{6} - \frac{D_i}{h_i}\right)\phi_{i-1/2} = \frac{h_{i+1}}{2}\langle q\rangle_{L,i+1} + \frac{h_i}{2}\langle q\rangle_{R,i} \ . \tag{2.10}$$

This system can be solved to get ϕ at each face. To allow for the use of lumped or standard LD in these equations, we introduce the factor θ, with $\theta = 1/3$ for standard

LD, and $\theta = 1$ for lumped LD. The diffusion equation becomes

$$\left(\frac{\sigma_{a,i+1}h_{i+1}}{4}(1-\theta) - \frac{D_{i+1}}{h_{i+1}}\right)\phi_{i+3/2} + \left(\frac{D_{i+1}}{h_{i+1}} + \frac{D_i}{h_i} + \left(\frac{1+\theta}{2}\right)\left[\frac{\sigma_{a,i+1}h_{i+1}}{2} + \frac{\sigma_{a,i}h_i}{2}\right]\right)\phi_{i+1/2} + \left(\frac{\sigma_{a,i}h_i}{4}(1-\theta) - \frac{D_i}{h_i}\right)\phi_{i-1/2} = \frac{h_{i+1}}{2}\langle q\rangle_{L,i+1} + \frac{h_i}{2}\langle q\rangle_{R,i} \ . \quad (2.11)$$

2.2.1.1 Boundary Conditions

The LO system exactly satisfies the inflow boundary conditions, therefore we choose a vacuum boundary condition for the left-most cell. The equation for the left moment at the first cell is given by

$$J_1 - J_{1/2} + \frac{\sigma_{a,i}h_i}{2}\left(\frac{1+\theta}{2}\phi_{L,i} + \frac{1-\theta}{2}\phi_{R,i}\right) = \frac{h_i}{2}\langle q\rangle_{L,i} \ , \quad (2.12)$$

The Marshak boundary condition for the vacuum inflow at face $x_{1/2}$ is given as

$$J^+_{1/2} = 0 = \frac{\phi_{1/2}}{4} + \frac{J_{1/2}}{2}, \quad (2.13)$$

which can be solved for $J_{1/2}$. Substitution of the above equation and Eq. (2.9) into Eq. (2.12) gives

$$\left(\frac{1}{2} + \sigma_{a,1}h_1\frac{1+\theta}{4} - \frac{D_1}{h_1}\right)\phi_{1/2} + \left(\sigma_{a,1}h_1\frac{1-\theta}{4} - \frac{D_1}{h_1}\right)\phi_{3/2} = \frac{h_i}{2}\langle q\rangle_{L,1} \quad (2.14)$$

a similar expression can be derived for the last cell.

2.2.2 Mapping Solution onto LD Unknowns

Solution of the continuous diffusion equation in the previous section provides correction values for ϕ on the faces, denoted as $\phi^C_{i+1/2}$. We now need to determine the correction these results provide for the LD representation of ϕ. To do this, first we

take the L and R finite element moments of the P_1 equations. A LDFE dependence is assumed on the interior of the cell for J and ϕ. Taking moments of Eq. (2.1) and simplifying yields

$$J_{i+1/2} - \frac{J_{L,i} + J_{R,i}}{2} + \frac{\sigma_{a,i} h_i}{2} \left(\frac{1}{3} \phi_{L,i} + \frac{2}{3} \phi_{R,i} \right) = \frac{h_i}{2} \langle q \rangle_{R,i} \tag{2.15}$$

$$\frac{J_{L,i} + J_{R,i}}{2} - J_{i-1/2} + \frac{\sigma_{a,i} h_i}{2} \left(\frac{2}{3} \phi_{L,i} + \frac{1}{3} \phi_{R,i} \right) = \frac{h_i}{2} \langle q \rangle_{L,i} \tag{2.16}$$

The moment equations for Eq. (2.2) are

$$\frac{1}{3} \left(\phi_{i+1/2} - \frac{\phi_{i,L} + \phi_{i,R}}{2} \right) + \frac{\sigma_{t,i} h_i}{2} \left(\frac{1}{3} J_{L,i} + \frac{2}{3} J_{R,i} \right) = 0 \tag{2.17}$$

$$\frac{1}{3} \left(\frac{\phi_{i,L} + \phi_{i,R}}{2} - \phi_{i-1/2} \right) + \frac{\sigma_{t,i} h_i}{2} \left(\frac{2}{3} J_{L,i} + \frac{1}{3} J_{R,i} \right) = 0 \tag{2.18}$$

Using similar equation for all the inflow currents, the balance equations for ϕ become The face terms $J_{i\pm1/2}$ and $\phi_{i\pm1/2}$ need to be eliminated from the system. The scalar flux is assumed to be the value provided by the continuous diffusion solution at each face, i.e., $\phi_{i\pm1/2} = \phi^C_{i\pm1/2}$. The currents are decomposed into half-range values to decouple the equations between cells. At $x_{i+1/2}$, the current is composed as $J_{i+1/2} = J^+_{i+1/2} - J^-_{i+1/2}$, where $+$ and $-$ denote the positive and negative half ranges of μ, respectively. Typically, the incoming current $J^-_{i+1/2}$ is upwinded from cell $i+1$. However, we approximate the incoming current based on $\phi^C_{i+1/2}$. The P_1 approximation provides the following relation

$$\phi = 2(J^+ + J^-). \tag{2.19}$$

At $x_{i+1/2}$, the above expression is solved for the incoming current $J^-_{i+1/2}$. The total

current becomes, with $\phi_{i+1/2} = \phi^C_{i+1/2}$,

$$J_{i+1/2} = J^+_{i+1/2} - J^-_{i+1/2} = 2J^+_{i+1/2} - \frac{\phi^C_{i+1/2}}{2}, \tag{2.20}$$

In the positive direction, at the right face, the values of ϕ and J are based on the LD representation within the cell at that face, i.e., $\phi_{R,i}$ and $J_{R,i}$. The standard P_1 approximation for the half-range currents and fluxes are used[22], i.e.,

$$J^\pm = \frac{\gamma\phi}{2} \pm \frac{J}{2}, \tag{2.21}$$

where γ accounts for the difference between the LO parameters and the true P_1 approximation. Thus, for the right face and positive half-range,

$$J^+_{i+1/2} = \frac{\gamma}{2}\phi_{i,R} + \frac{J_{i,R}}{2} \tag{2.22}$$

A similar expression can be derived for $x_{i-1/2}$. The total currents at each face are thus

$$J_{i+1/2} = \gamma\phi_{i,R} + J_{i,R} - \frac{\phi^C_{i+1/2}}{2} \tag{2.23}$$

$$J_{i-1/2} = \frac{\phi^C_{i-1/2}}{2} - \gamma\phi_{i,L} + J_{i,L} \tag{2.24}$$

Substitution of these results back into the LD balance equations and introduction of the lumping notation yields the final equations

$$\left(\gamma\phi_{i,R} + J_{i,R} - \frac{\phi^C_{i+1/2}}{2}\right) - \frac{J_{L,i} + J_{R,i}}{2} + \frac{\sigma_{a,i}h_i}{2}\left(\frac{(1-\theta)}{2}\phi_{L,i} + \frac{(1+\theta)}{2}\phi_{R,i}\right) = \frac{h_i}{2}\langle q\rangle_{R,i} \tag{2.25}$$

$$\frac{J_{L,i}+J_{R,i}}{2}-\left(\frac{\phi^C_{i-1/2}}{2}-\gamma\phi_{i,L}+J_{i,L}\right)+\frac{\sigma_{a,i}h_i}{2}\left(\frac{(1+\theta)}{2}\phi_{L,i}+\frac{(1-\theta)}{2}\phi_{R,i}\right)=\frac{h_i}{2}\langle q\rangle_{L,i} \tag{2.26}$$

$$\frac{1}{3}\left(\phi^C_{i+1/2}-\frac{\phi_{i,L}+\phi_{i,R}}{2}\right)+\frac{\sigma_{t,i}h_i}{2}\left(\frac{(1-\theta)}{2}J_{L,i}+\frac{(1+\theta)}{2}J_{R,i}\right)=0 \tag{2.27}$$

$$\frac{1}{3}\left(\frac{\phi_{i,L}+\phi_{i,R}}{2}-\phi^C_{i-1/2}\right)+\frac{\sigma_{t,i}h_i}{2}\left(\frac{(1+\theta)}{2}J_{L,i}+\frac{(1-\theta)}{2}J_{R,i}\right)=0. \tag{2.28}$$

The above equations are completely local to each cell and fully defined. The system can be solved for the the desired unknowns $\phi_{i,L}$, $\phi_{i,R}$, $J_{i,L}$, and $J_{i,R}$.

2.2.3 DSA Source Definition

The above discretization procedure is used to determine the error in the scalar flux. The sources $\langle q\rangle_{L/R}$ thus need to be defined. They are simply the residual in the scattering iterations, given by

$$q=\sigma_s\left(\phi^{l+1/2}-\phi^l\right). \tag{2.29}$$

The spatial moments are straight forward:

$$\langle q\rangle_{L,i}=\sigma_{s,i}\left(\langle\phi^{l+1/2}\rangle_{L,i}-\langle\phi^l\rangle_{L,i}\right) \tag{2.30}$$

The above equation is valid for lumping or standard LD. This is because the LO moments are defined differently for LLD or LD, resulting in equations that are consistent. For instance, for lumped LD, the LO system uses the spatial closure that the edge value is defined as the moment, i.e., $\langle\phi\rangle_{R,i}\equiv\phi_{R,i}$. For a standard lumped source, we desire the right equation to have $\langle q\rangle_{R,i}=\sigma_s(\phi^{l+1/2}_{R,i}-\phi^l_{R,i})$. Substituting

the lumped closure into the right hand side of this equation gives back the original equation, i.e., $\langle q \rangle_{R,i} = \sigma_{s,i} \left(\langle \phi^{l+1/2} \rangle_{R,i} - \langle \phi^{l} \rangle_{R,i} \right)$. The same is true for standard LD.

2.2.4 Updating the LO Unkowns

We now have a correction to J and ϕ for the volumetric finite element unknowns. Because we are interested in the time-dependent solution, we need to accelerate the solution for the half-range fluxes, rather than just the scalar flux. We only accelerate the zeroth moment of the angular intensity. The error in the scalar intensities are defined as

$$\delta\phi^{\pm} = \frac{\delta\phi}{2} \pm \frac{3\delta J}{4} \tag{2.31}$$

Spatial moments are taken of $\delta\phi^{\pm}$, using the lumping notation of LD on the interior

$$\langle \delta\phi^{\pm} \rangle_L = \frac{1+\theta}{2}\delta\phi_L^{\pm} + \frac{1-\theta}{2}\delta\phi_R^{\pm} \tag{2.32}$$

$$\langle \delta\phi^{\pm} \rangle_R = \frac{1-\theta}{2}\delta\phi_L^{\pm} + \frac{1+\theta}{2}\delta\phi_R^{\pm}, \tag{2.33}$$

where Eq. (2.31) can be used to get in terms of $\delta\phi_{L/R}$ and $\delta J_{L/R}$. It is noted that for consistency, the updates to the moments depend on the lumping notation, even though the sources are defined the same in both cases.

REFERENCES

[1] S.R. Bolding and J.E. Morel. A High-Order Low-Order Algorithm with Exponentially-Convergent Monte Carlo for k-Eigenvalue problems. ANS Winter Meeting. Anaheim, CA, 2014.

[2] Subrahmanyan Chandrasekhar. *Radiative Transfer*. Courier Corporation, 2013.

[3] Jeffery D. Densmore. Asymptotic analysis of the spatial discretization of radiation absorption and re-emission in implicit monte carlo. *Journal of Computational Physics*, 230(4):1116 – 1133, 2011.

[4] Jeffery D. Densmore and Edward W. Larsen. Asymptotic equilibrium diffusion analysis of time-dependent monte carlo methods for grey radiative transfer. *Journal of Computational Physics*, 199(1):175 – 204, 2004.

[5] Jeffery D Densmore, Kelly G Thompson, and Todd J Urbatsch. A hybrid transport-diffusion monte carlo method for frequency-dependent radiative-transfer simulations. *Journal of Computational Physics*, 231(20):6924–6934, 2012.

[6] Paul Nelson Edward W. Larsen. Finite-difference approximations and superconvergence for the discrete-ordinate equations in slab geometry. *SIAM Journal on Numerical Analysis*, 19(2):334–348, 1982.

[7] Edward W. Larsen and Jim E. Morel. Advances in discrete-ordinates methodology. *Nuclear Computational Science. Springer Netherlands*, pages 1–84, 2010.

[8] J. A. Fleck, Jr. and J. D. Cummings, Jr. An implicit monte carlo scheme for calculating time and frequency dependent nonlinear radiation transport. *J. Comput. Phys.*, 8(3):313–342, December 1971.

[9] N. A. Gentile and Ben C. Yee. Iterative implicit monte carlo. *Journal of Computational and Theoretical Transport*, 0(0):1–31, 0.

[10] NA Gentile. Implicit monte carlo diffusion: An acceleration method for monte carlo time-dependent radiative transfer simulations. *Journal of Computational Physics*, 172(2):543–571, 2001.

[11] Eugene D. Brooks III, Michael Scott McKinley, Frank Daffin, and Abraham Szke. Symbolic implicit monte carlo radiation transport in the difference formulation: a piecewise constant discretization. *Journal of Computational Physics*, 205(2):737 – 754, 2005.

[12] Eugene D. Brooks III, Abraham Szke, and Jayson D.L. Peterson. "piecewise linear discretization of symbolic implicit monte carlo radiation transport in the difference formulation ". *"Journal of Computational Physics "*, "220"(1):471 – 497, 2006.

[13] Rong Kong and Jerome Spanier. A new proof of geometric convergence for general transport problems based on sequential correlated sampling methods. *Journal of Computational Physics*, 227:9762 – 9777, 2008.

[14] Edward W. Larsen, Akansha Kumar, and Jim E. Morel. Properties of the implicitly time-differenced equations of thermal radiation transport. *J. Comput. Phys.*, 238:82–96, April 2013.

[15] E.W. Larsen, G.C. Pomraning, and V.C. Badham. Asymptotic analysis of radiative transfer problems. *Journal of Quantitative Spectroscopy and Radiative Transfer*, 29(4):285 – 310, 1983.

[16] Elmer Eugene Lewis and Warren F Miller. *Computational methods of neutron transport*. John Wiley and Sons, Inc., New York, NY, 1984.

[17] Michael Scott McKinley, Eugene D Brooks III, and Abraham Szoke. Comparison of implicit and symbolic implicit monte carlo line transport with frequency weight vector extension. *Journal of Computational Physics*, 189(1):330–349, 2003.

[18] J.E. Morel, T.A. Wareing, and K. Smith. Linear-Discontinuous Spatial Differencing Scheme for S_n Radiative Transfer Calculations. *Journal of Computational Physics*, 128:445–462, 1996.

[19] H. Park, J.D. Densmore, A.B. Wollaber, D.A. Knoll, and R.M. Ramenzahn. Monte Carlo Solution Methods in a Moment-Based Scale-Bridging Algorithm For Thermal Radiative Transfer Problems. M&C. Sun Valley, ID, 2013.

[20] J.R. Peterson. Exponentially Convergent Monte Carlo for the 1-d Transport Equation. Master's thesis, Texas A&M, 2014.

[21] J.K. Shultis and W.L. Dunn. *Exploring Monte Carlo Methods*. Academic Press, Burlington, MA 01803, 2012.

[22] "Weston M. Stacey". *"Nuclear Reactor Physics"*. Wiley, 2007.

[23] T.A. Wareing. *Asymptotic diffusion accelerated discontinuous finite element methods for transport problems*. PhD thesis, Michigan, 1991.

[24] T.A. Wareing, E.W. Larsen, and M.L. Adams. Asymptotic Diffusion Accelerated Discontinuous Finite Element Schemes for the S_N Equations in Slab and X-Y Geometries. In *International Topical Meeting on Advances in Mathematics, Computations, Reactor Physics*, volume 3, Pittsburgh, PA, 1991.

[25] J. Willert, C.T. Kelly, D.A. Knoll, and H. Park. A Hybrid Approach to the Neutron Transport k-Eigenvalue Problem using NDA-based Algorithms. M&C. Sun Valley, ID, 2013.

[26] Jeffrey Willert and H. Park. Residual monte carlo high-order solver for moment-based accelerated thermal radiative transfer equations. *Journal of Computational Physics*, 276:405 – 421, 2014.

[27] Allan B Wollaber, Edward W Larsen, and Jeffery D Densmore. A discrete maximum principle for the implicit monte carlo equations. *Nuclear Science and Engineering*, 173(3):259–275, 2013.

[28] E.R. Wolters. *Hybrid Monte Carlo - Deterministic Neutron Transport Methods Using Nonlinear Functionals*. PhD thesis, Michigan, 2011.

APPENDIX A

FIRST APPENDIX

Text for the Appendix follows.

Figure A.1: TAMU figure

APPENDIX B

SECOND APPENDIX WITH A LONGER TITLE - MUCH LONGER IN FACT

Text for the Appendix follows.

Figure B.1: TAMU figure

B.1 Appendix Section